

Supplementary Material for “Large collective Lamb shift of two distant superconducting artificial atoms”

P. Y. Wen,^{1,2,*} K.-T. Lin,^{3,*} A. F. Kockum,^{4,5,*} B. Suri,^{6,4} H. Ian,^{7,8} J. C. Chen,^{1,2}
 S. Y. Mao,⁹ C. C. Chiu,¹⁰ P. Delsing,⁴ F. Nori,^{5,11} G.-D. Lin,³ and I.-C. Hoi^{1,2,†}

¹*Department of Physics, National Tsing Hua University, Hsinchu 30013, Taiwan*

²*Center for Quantum Technology, National Tsing Hua University, Hsinchu 30013, Taiwan*

³*Department of Physics, National Taiwan University, Taipei 10617, Taiwan*

⁴*Department of Microtechnology and Nanoscience,*

Chalmers University of Technology, 412 96 Gothenburg, Sweden

⁵*Theoretical Quantum Physics Laboratory, RIKEN Cluster for Pioneering Research, Wako-shi, Saitama 351-0198, Japan*

⁶*Department of Instrumentation and Applied Physics,
 Indian Institute of Science, Bengaluru 560012, India*

⁷*Institute of Applied Physics and Materials Engineering, University of Macau, Macau*

⁸*UMacau Zhuhai Research Institute, Zhuhai, Guangdong, China*

⁹*Institute of Electro-Optical Engineering, National Chiao Tung University, Hsinchu 30013, Taiwan*

¹⁰*Department of Electrical Engineering, National Tsing Hua University, Hsinchu 30013, Taiwan*

¹¹*Physics Department, The University of Michigan, Ann Arbor, Michigan 48109-1040, USA*

(Dated: September 23, 2019)

CONTENTS

S1. Derivation of master equation and qubit-qubit interaction	1
S2. Reflection coefficient	3
A. General derivation	3
B. Effect of dephasing on the reflection for two qubits	3
S3. Full spectroscopy	4
S4. Additional information for figures in the main text	5
References	5

S1. DERIVATION OF MASTER EQUATION AND QUBIT-QUBIT INTERACTION

In this section, we outline the derivation of qubit-qubit coupling through virtual photons in the continuum of photonic modes in a 1D transmission line terminated by a mirror [S1]. We consider N transmon qubits, placed at positions x_n in the transmission line. The coordinate x_n measures the distance from qubit n to the mirror at $x = 0$. The Hamiltonian for this system can be expressed as $H = H_S + H_B + H_{\text{int}}$ with

$$H_S = \sum_{n=1}^N \hbar\omega_{10}^n \sigma_n^+ \sigma_n^-, \quad (\text{S1})$$

$$H_B = \int d\omega \hbar\omega a_\omega^\dagger a_\omega, \quad (\text{S2})$$

$$H_{\text{int}} = i \sum_{n=1}^N \int d\omega \hbar g_n(\omega) \cos(k_\omega x_n) (a_\omega \sigma_n^+ - \sigma_n^- a_\omega^\dagger). \quad (\text{S3})$$

Here, H_S is the bare Hamiltonian of the qubits, with σ_n^+ (σ_n^-) the raising (lowering) operator of qubit n and ω_{10}^n the transition frequency of qubit n . The bare Hamiltonian for the continuum of photonic modes in the transmission

* These authors contributed equally

† e-mail: ichoi@phys.nthu.edu.tw

line is given by H_B , where a_ω^\dagger (a_ω) is the creation (annihilation) operator for excitations at mode frequency ω . The interaction between the qubits and the photons is described by H_{int} , where the interaction strength is given by [S2]

$$g_n(\omega) = e\beta_n \left(\frac{E_J^{(n)}}{8E_C^{(n)}} \right)^{1/4} \sqrt{\frac{2Z_0\omega}{\hbar\pi}}, \quad (\text{S4})$$

where $\beta_n = C_c^n/C_\Sigma^n$ is the ratio between the coupling capacitance C_c^n to the transmission line and the qubit capacitance C_Σ^n for qubit n , $E_C^{(n)}$ and $E_J^{(n)}$ are the charging and Josephson energies, respectively, of qubit n , e is the elementary charge, and Z_0 is the characteristic impedance for the transmission line. The cosine function in H_{int} reflects the presence of a mirror giving an open boundary condition at $x = 0$.

Using the standard procedure of eliminating the photonic degrees of freedom under the Born-Markov approximation [S3], we obtain the interaction-picture master equation

$$\begin{aligned} \frac{d\rho}{dt} = & i \sum_{n=1}^N \delta_n [\sigma_n^+ \sigma_n^-, \rho] + i \sum_{n=1}^N \Omega_p^n \cos(k_p x_n) [\sigma_n^x, \rho] - i \sum_{n \neq m=1}^N (\Delta_{nm}^+ - i\Gamma_{nm}^-) [\sigma_n^+ \sigma_m^-, \rho] \\ & + \sum_{n,m=1}^N (\Gamma_{nm}^+ + i\Delta_{nm}^-) (2\sigma_m^- \rho \sigma_n^+ - \sigma_n^+ \sigma_m^- \rho - \rho \sigma_n^+ \sigma_m^-) + \sum_{n=1}^N \gamma_{\phi_n} (2\sigma_n^+ \sigma_n^- \rho \sigma_n^+ \sigma_n^- - \sigma_n^+ \sigma_n^- \rho - \rho \sigma_n^+ \sigma_n^-), \end{aligned} \quad (\text{S5})$$

where the qubit-qubit interaction is determined by

$$\Gamma_{nm}^+ = \frac{\gamma_{nm} + \gamma_{mn}}{2}, \quad (\text{S6})$$

$$\Gamma_{nm}^- = \frac{\gamma_{nm} - \gamma_{mn}}{2}, \quad (\text{S7})$$

$$\Delta_{nm}^+ = \frac{\Delta_{nm} + \Delta_{mn}}{2}, \quad (\text{S8})$$

$$\Delta_{nm}^- = \frac{\Delta_{nm} - \Delta_{mn}}{2}, \quad (\text{S9})$$

with

$$\gamma_{nm} = \frac{\pi\alpha_{nm}\omega_{10}^m}{2} \{ \cos(k_m[x_n + x_m]) + \cos(k_m|x_n - x_m|) \}, \quad (\text{S10})$$

$$\Delta_{nm} = \frac{\pi\alpha_{nm}\omega_{10}^m}{2} \{ \sin(k_m[x_n + x_m]) + \sin(k_m|x_n - x_m|) \}, \quad (\text{S11})$$

$$\alpha_{nm} = \frac{2\beta_n\beta_m e^2 Z_0}{\hbar\pi} \left(\frac{E_J^{(n)}}{8E_C^{(n)}} \right)^{1/4} \left(\frac{E_J^{(m)}}{8E_C^{(m)}} \right)^{1/4}. \quad (\text{S12})$$

In these expressions, the subscripts n and m refer to qubits n and m ; in general, these indices are not interchangeable in terms where they occur together if the two qubits they refer to are non-identical. The first term in Eq. (S5) is the Hamiltonian for the individual qubits. Here, we have absorbed single-qubit Lamb shifts into the detuning δ_n between the frequency of qubit n and the frequency ω_p of a probe field:

$$\delta_n = \omega_p - \omega_n - \Delta_{nn}. \quad (\text{S13})$$

The second term in Eq. (S5) is the Hamiltonian showing qubit n is driven by the probe field, which is characterized by the Rabi frequency

$$\hbar\Omega_p^n = 2\sqrt{2}e\beta_n \left(\frac{E_J^{(n)}}{8E_C^{(n)}} \right)^{1/4} V_0, \quad (\text{S14})$$

where V_0 is the input voltage. The third term in Eq. (S5) is the qubit-qubit interaction that gives rise to the collective Lamb shift. The fourth term in Eq. (S5) describes individual and collective relaxation processes for the qubits. We note that the individual bare decay rate for qubit n is given by

$$\gamma_n = \pi g_n^2(\omega_{10}^n) = \pi\alpha_{nn}\omega_{10}^n. \quad (\text{S15})$$

Finally, the fifth term in Eq. (S5) describes pure dephasing. The pure dephasing rate of qubit n is γ_{ϕ_n} .

S2. REFLECTION COEFFICIENT

A. General derivation

In this section, we summarize the calculation for obtaining the reflection coefficient

$$r \equiv |V_{\text{out}}/V_{\text{in}}| \quad (\text{S16})$$

from the qubits in the semi-infinite transmission line for an input voltage V_{in} . The output voltage is given by

$$V_{\text{out}}(x, t) = V_{\text{in}}(x, t) + V_{\text{s}}(x, t), \quad (\text{S17})$$

where the scattered signal is

$$V_{\text{s}}(x, t) = -i\sqrt{\frac{\hbar Z_0}{4\pi}} \int_0^\infty d\omega \sqrt{\omega} a_\omega(t) e^{ikx}. \quad (\text{S18})$$

Here, the photonic operator $a_\omega(t) = \tilde{a}_\omega(t)e^{-i\omega t}$ can be expressed in terms of the slowly varying amplitude

$$\tilde{a}_\omega(t) = -\sum_{n=1}^N g_n(\omega) \int_0^t \tilde{\sigma}_n^-(s) e^{i(\omega - \omega_n)s} ds, \quad (\text{S19})$$

with $\tilde{\sigma}_n^-(t) = \sigma_n(t)e^{i\omega_n t}$. Substituting \tilde{a}_ω into V_{s} and performing the integration, we obtain

$$V_{\text{s}}(x, t) = i \sum_{n=1}^N \sqrt{2} e \beta_n Z_0 \omega_n \left(\frac{E_{\text{J}}^{(n)}}{8E_{\text{C}}^{(n)}} \right)^{1/4} \cos(k_{\text{p}} x_n) \tilde{\sigma}_n^-(t). \quad (\text{S20})$$

Since the input signal V_{in} is connected to the Rabi frequency of the pumping field through Eq. (S14) by taking $n = N$, we immediately obtain

$$r = \left| 1 + i \sum_m \frac{4\eta_{Nm}\gamma_m}{\Omega_{\text{P}}^N} \cos(k_{\text{p}} x_m) \langle \sigma_m^- \rangle \right|, \quad (\text{S21})$$

with

$$\eta_{Nm} = \frac{\beta_N}{\beta_m} \left(\frac{E_{\text{J}}^{(N)} E_{\text{C}}^{(m)}}{E_{\text{J}}^{(m)} E_{\text{C}}^{(N)}} \right)^{1/4}. \quad (\text{S22})$$

The reflection coefficient can then be computed numerically by evolving the master equation in Eq. (S5).

B. Effect of dephasing on the reflection for two qubits

In our experiment, we only have $N = 2$ qubits. In this section, we investigate the behaviour of the reflection coefficient r in greater detail for this case. In particular, we elucidate how the extinction of signal away from the anti-crossings in Fig. 3 (a), (b) in the main text arises. To understand how r depends on various parameters, we recast the master equation [Eq. (S5)] into an effective Hamiltonian, yielding [S1]

$$H_{\text{eff}}/\hbar = -\sum_{n=1}^N \delta_n \sigma_n^+ \sigma_n^- - \sum_{n=1}^N \Omega_{\text{p}} \cos(k_{\text{p}} x_i) \sigma_n^x + \sum_{n \neq m=1}^N (\Delta_{nm} - i\gamma_{nm}) \sigma_n^+ \sigma_m^- - i \sum_{n=1}^N \gamma_n^\phi \sigma_n^+ \sigma_n^-. \quad (\text{S23})$$

For the case $N = 2$, with the first qubit located at x_1 on resonance with the probe ($\delta_1 = 0$) and the second qubit located at the mirror, i.e., $x_2 = 0$, we plug in explicit parameters and obtain

$$H_{\text{eff}}/\hbar = \gamma_0 \sin \theta_1 \cos \theta_1 \sigma_1^+ \sigma_1^- - \delta_2 \sigma_2^+ \sigma_2^- - \Omega_{\text{p}} (\cos \theta_1 \sigma_1^x + \sigma_2^x) + \gamma_0 \sin \theta_1 \sigma_2^+ \sigma_1^- + \gamma_0 \sin \theta_2 \sigma_1^+ \sigma_2^- \\ - i(\gamma_0 \cos^2 \theta_1 + \gamma_{\phi_1}) \sigma_1^+ \sigma_1^- - i(\gamma_0 + \gamma_{\phi_2}) \sigma_2^+ \sigma_2^- - i\gamma_0 \cos \theta_1 \sigma_2^+ \sigma_1^- - i\gamma_0 \cos \theta_2 \sigma_1^+ \sigma_2^- \quad (\text{S24})$$

where γ_0 and $\delta_2 \equiv \omega_p - \omega_2$ are the spontaneous decay rate and probe detuning, respectively, of the mirror qubit. The phases $\theta_1 = k_p x_1$ and $\theta_2 = \omega_2 x_1 / v$ are due to the distance from Qubit 1 to the mirror, measured by frequencies resonant with Qubit 1 and Qubit 2, respectively.

We assume the two-qubit state to be of the form

$$|\psi\rangle \equiv C_{ee}|ee\rangle + C_{eg}|eg\rangle + C_{ge}|ge\rangle + C_{gg}|gg\rangle, \quad (\text{S25})$$

where $|s_1 s_2\rangle$ denotes state $|s_1\rangle_{\text{distant}} \otimes |s_2\rangle_{\text{mirror}}$ with $s_1, s_2 = e, g$. Under this assumption, and also assuming that the probe field is weak ($\Omega_p \ll \gamma_0$), the steady-state solution to the Schrödinger equation

$$i\hbar \frac{d}{dt} |\psi\rangle = H_{\text{eff}} |\psi\rangle \quad (\text{S26})$$

is given by $c_{gg} \approx 1$, $c_{ee} \approx \mathcal{O}([\Omega_p/\gamma_0]^2)$, and

$$C_{eg} \simeq i \frac{\Omega_p}{\gamma_0} \left[e^{-i\theta_1} - \frac{e^{-2i\theta_1}}{\gamma_0} \frac{(\gamma_0 - i\delta_2)}{(\gamma_0 - i\delta_2) \cos \theta_1 - \gamma_0 e^{i\theta_2}} \gamma_{\phi_1} \right], \quad (\text{S27})$$

$$C_{ge} \simeq i \frac{\Omega_p}{\gamma_0} \frac{e^{-i\theta_1}}{(\gamma_0 - i\delta_2) \cos \theta_1 - \gamma_0 e^{i\theta_2}} \gamma_{\phi_1}. \quad (\text{S28})$$

Here, we have also treated the pure dephasing rates γ_{ϕ_i} perturbatively compared to γ_0 , and only kept terms up to first order in γ_{ϕ_i}/γ_0 . Note that γ_{ϕ_2} does not explicitly play a role at these orders.

The reflection amplitude is now given by

$$|r| = \left| 1 + i \sum_n \frac{2\gamma_0}{\Omega_p} \cos \phi_n |\sigma_n^- \rangle \right| = \left| 1 + i \frac{2\gamma_0}{\Omega_p} (\cos \theta_1 C_{eg} + C_{ge}) \right|, \quad (\text{S29})$$

which can be written on the form $|u_0 + u_1 \frac{\gamma_{\phi_1}}{\gamma_0}|$. It can be shown that

$$u_0 = 1 - 2e^{-i\theta_1} \cos \theta_1 = -e^{2i\theta_1} \quad (\text{S30})$$

corresponds to the case without pure dephasing, where $|r| = |u_0| = 1$ for any θ . For finite γ_{ϕ_1} , the leading-order correction u_1 is given by

$$u_1 = -2ie^{-2i\theta_1} \left(\frac{\delta_2 \cos \theta_1 + \gamma_0 \sin \theta_1}{(\gamma_0 - i\delta_2) \cos \theta_1 - \gamma_0 e^{i\theta_2}} \right), \quad (\text{S31})$$

which leads to $|r|$ dropping below unity.

At the anticrossing in Fig. 3 (a), (b) in the main text, u_1 goes to zero since both δ_2 and θ_1 go to zero. However, u_1 may also vanish when the following condition is fulfilled:

$$\delta_2 = -\gamma_0 \tan \theta_1, \quad (\text{S32})$$

with $\theta_1 = k_p x_1 = (\omega_2 + \delta_2)x_1/v$. In our setup, $x_1 = 33$ mm, and $v = 0.893 \times 10^8$ m/s. In the case when the distant qubit is located at $x_1 = \frac{7}{4}\lambda_2$ ($\lambda_2 \equiv \frac{2\pi v}{\omega_2}$), and $\omega_2 = 2\pi \times 4.75$ GHz, we obtain the ‘‘discontinuity’’ ($|r| \rightarrow 1$) in the reflection amplitude curves at $\delta_2 = -0.12$ GHz and 0.10 GHz by solving Eq. (S32). These are the points where the signal is extinguished away from the anti-crossing, along the diagonal, in Fig. 3 (a), (b) in the main text.

S3. FULL SPECTROSCOPY

In this section, we present the full data from the single-qubit spectroscopy, part of which was shown in Fig. 2 in the main text. Figure S1 shows the amplitude reflection coefficient $|r|$ as a function of probe frequency ω_p and qubit frequency in the full range 4 – 8 GHz, which is the bandwidth of the cryogenic low-noise amplifier in our experimental setup. As explained in the caption, we use this data to extract the speed of light in the transmission line.

In each of our transmon qubits, two capacitively shunted Josephson junctions form a SQUID loop. The external flux Φ through this loop affects the transition energy of the qubit [S4]:

$$\hbar\omega_{10}(\Phi) \approx \sqrt{8E_J(\Phi)E_C} - E_C. \quad (\text{S33})$$

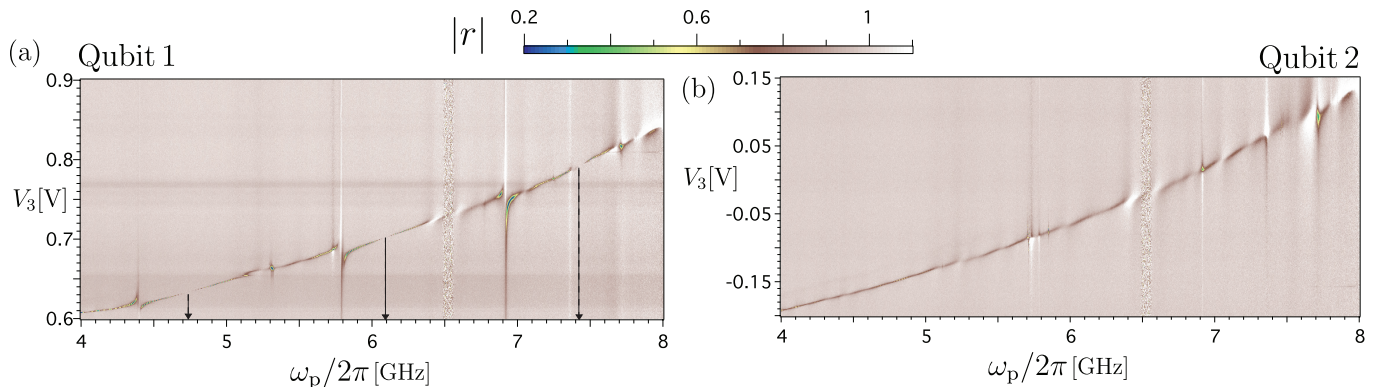


Figure S1. Amplitude reflection coefficient $|r|$ as a function of probe frequency ω_p and a magnetic flux tuning the qubit frequencies for the full bandwidth of our measurement setup. In each measurement, the other qubit is detuned far from resonance. (a) The data for Qubit 1, which is located away from the mirror. The dashed arrows indicate frequencies where the response shows that Qubit 1 sits at a node for the electromagnetic field in the transmission line. The marked frequencies are $f_1 = 4.745$ GHz, $f_2 = 6.094$ GHz, and $f_3 = 7.414$ GHz; they correspond to $L = 7\lambda_1/4$, $L = 9\lambda_2/4$, and $L = 11\lambda_3/4$, respectively. Knowing that $L = 33$ mm, this lets us calculate the speed of light in the transmission line. We find $v = f_1 \lambda_1 = 0.8948 \times 10^8$ m/s $\approx f_2 \lambda_2 \approx f_3 \lambda_3$. (b) The data for Qubit 2, which is located right by the mirror. In both (a) and (b), a number of anti-crossings can be seen. We attribute these anti-crossings to stray resonances interacting with the qubits. These stray resonances are most likely standing-wave modes formed between the mirror and bonding wires on the chip.

Qubit (Bias)	$\omega_{10}/2\pi$ [GHz]	$\Gamma_1/2\pi$ [MHz]	$\gamma_\phi/2\pi$ [MHz]	$\gamma/2\pi$ [MHz]
Q1 (A)	4.697	0.3	2.1	2.25
Q1 (B)	5.01	8	1.7	5.7
Q2 (C)	4.692	21	2.15	12.65
Q2 (D)	5.014	21	2	12.5

Table S1. Extracted parameters from the linecuts *A-D* in Fig. 2(e) and (f). The fit to theory is performed following Ref. [S5].

The transition energy is determined by the charging energy $E_C = e^2/2C_\Sigma$ and the Josephson energy

$$E_J(\Phi) = E_J |\cos(\pi\Phi/\Phi_0)|, \quad (\text{S34})$$

where $\Phi_0 = h/2e$ is the magnetic flux quantum. The Josephson energy can be tuned from its maximum value E_J by the external flux Φ via a magnetic coil or local flux line.

S4. ADDITIONAL INFORMATION FOR FIGURES IN THE MAIN TEXT

For completeness, we here present the parameters extracted from fitting the linecuts in the single-tone spectroscopy shown in Fig. 2(e) and (f) in the main text. These parameters are given in Table S1.

In Fig. S2, we show two examples of data and theoretical simulations of the avoided level crossing that appears when the qubits are tuned into resonance with each other at points that do not correspond to a node for Qubit 1. This is in contrast to Fig. 3 in the main text, which shows the anti-crossing when Qubit 1 is at a node. The data in Fig. S2 show that the CLS becomes hard or impossible to resolve when Qubit 1 is not at a node of the field in the TL.

Finally, we also provide the theoretical simulation of the experimental results presented in Fig. 4(a) in the main text. These simulations are shown in Fig. S3.

[S1] K.-T. Lin, T. Hsu, C.-Y. Lee, I.-C. Hoi, and G.-D. Lin, “Scalable collective Lamb shift of a 1D superconducting qubit array in front of a mirror,” (2019), arXiv:1905.04743.

[S2] I.-C. Hoi, A. F. Kockum, L. Tornberg, A. Pourkabirian, G. Johansson, P. Delsing, and C. M. Wilson, “Probing the quantum vacuum with an artificial atom in front of a mirror,” *Nat. Phys.* **11**, 1045 (2015), arXiv:1410.8840.

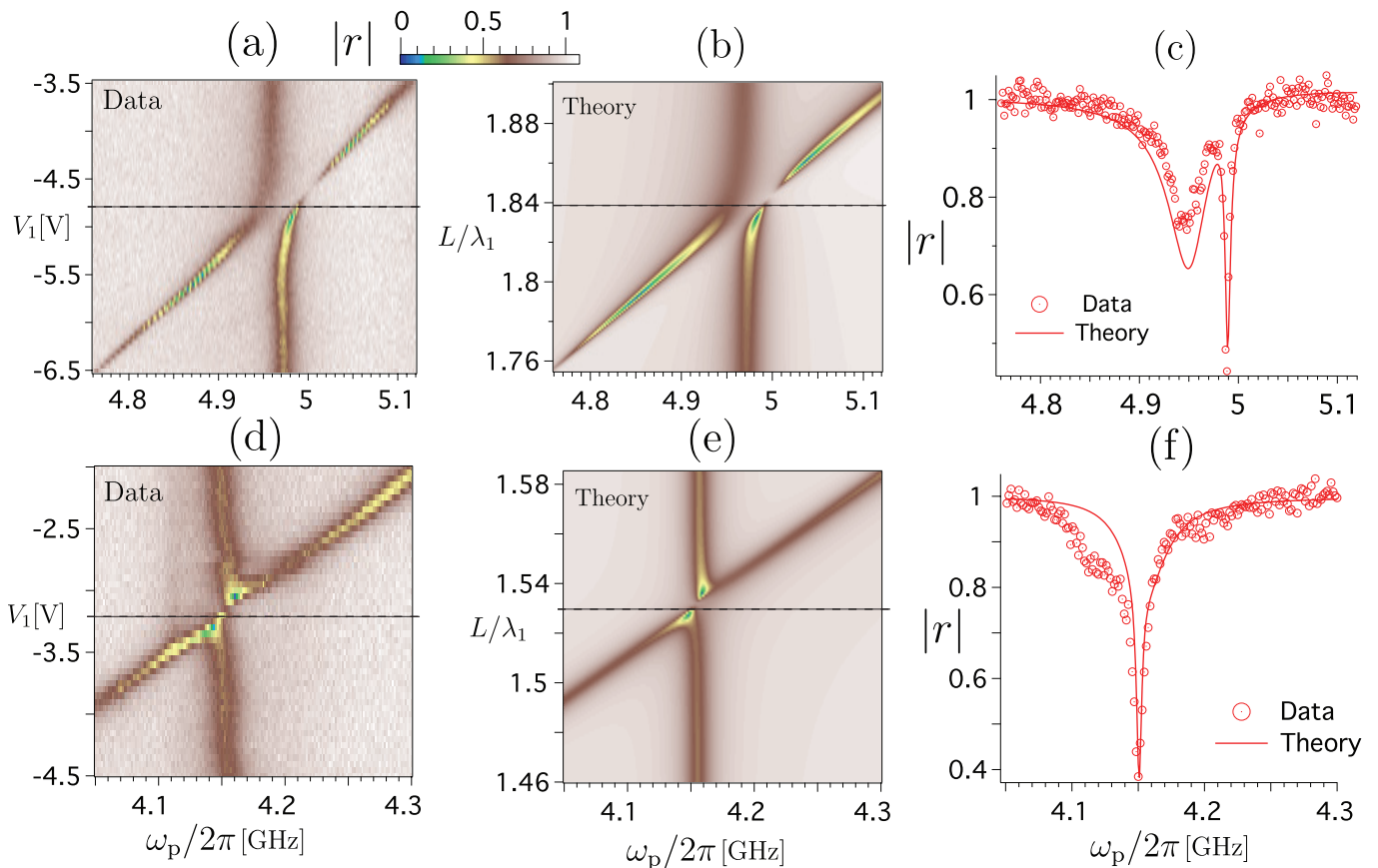


Figure S2. Collective Lamb shift with Qubit 1 tuned away from the node of the field in the TL. (a), (d) The amplitude reflection coefficient for a weak probe as a function of the probe frequency ω_p and the transition frequency of Qubit 1 (controlled through the voltage V_1). The frequency of Qubit 2 is fixed at $\omega_{10} = 4.95$ GHz in (a) and $\omega_{10} = 4.15$ GHz in (d), respectively. The frequency of Qubit 1 is tuned through resonance with this frequency. (b), (e) Theory simulation of the single-tone spectroscopy data in panels (a) and (d), respectively. For (b), the simulation is done with the same parameters as given in the caption of Fig. 3 in the main text. For (e), the data were taken on the same device, but in a different thermal cycle. For this simulation, the free parameters changed to $\beta_1 = 0.249$, $\beta_2 = 0.25$, and $\gamma_\phi/2\pi = 2$ MHz. The agreement between the data in (a) and (d) and the simulations in (b) and (e) is excellent. The extinction of the signal close to the anti-crossing in panels (a) and (b) is due to the same effect as in panels (a) and (b) in Fig. 3 in the main text. (c), (f) A linecut of the data and theory (marked by the dashed line in the preceding panels) at the point where the two qubits are on, or very close to, resonance. In panel (c), we see one broad and one narrow dip in the reflection; these dips correspond to the superradiant and subradiant states, respectively. In panels (d)-(f), we see that the Lamb shift can no longer be resolved over the decoherence of the qubits, since Qubit 1 now is too far from a node of the field to have its relaxation rate markedly suppressed.

[S3] H. J. Carmichael, *Statistical Methods in Quantum Optics 1* (Springer, 1999).

[S4] J. Koch, T. M. Yu, J. Gambetta, A. A. Houck, D. I. Schuster, J. Majer, A. Blais, M. H. Devoret, S. M. Girvin, and R. J. Schoelkopf, "Charge-insensitive qubit design derived from the Cooper pair box," *Phys. Rev. A* **76**, 042319 (2007), [arXiv:0703002 \[cond-mat\]](https://arxiv.org/abs/0703002).

[S5] I.-C. Hoi, A. F. Kockum, T. Palomaki, T. M. Stace, B. Fan, L. Tornberg, S. R. Sathyamoorthy, G. Johansson, P. Delsing, and C. M. Wilson, "Giant Cross-Kerr Effect for Propagating Microwaves Induced by an Artificial Atom," *Phys. Rev. Lett.* **111**, 053601 (2013), [arXiv:1207.1203](https://arxiv.org/abs/1207.1203).

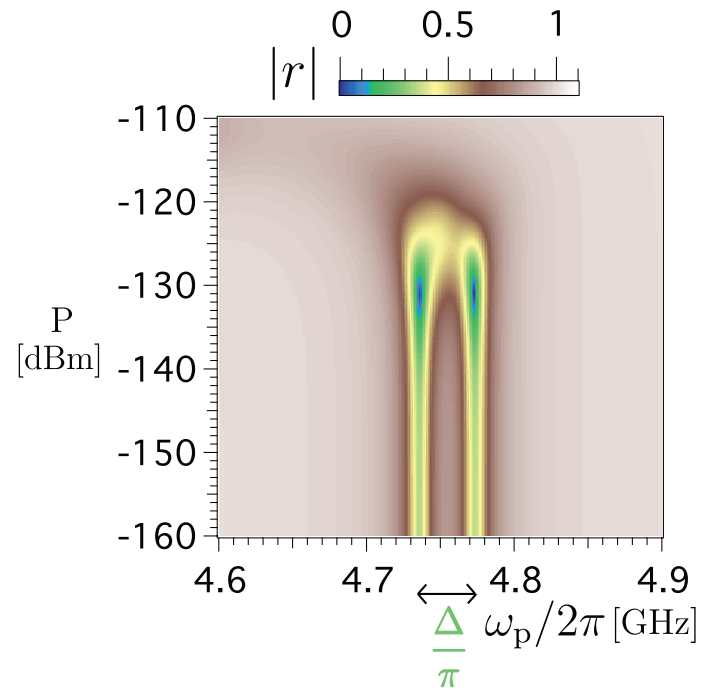


Figure S3. Theoretical simulation of the results in Fig. 4(a) in the main text. The simulation uses parameter values extracted in earlier measurements given in the main text.